EUROPEAN JOURNAL OF PURE AND APPLIED MATHEMATICS
2025, Vol. 18, Issue 3, Article Number 6302
ISSN 1307-5543 – ejpam.com
Published by New York Business Global

Green Synthesis of Silver Nanoparticles with *Musa Acuminata* Flower Extraction: A Fractional Approach

R. Dhanalakshmi[1,*], N. Jeeva[2,3], K.M. Dharmalingam[2], M.C. Kekana[4]

[1] *PG and Research Department of Physics, Thiagarajar College, Madurai, Tamil Nadu, India*
[2] *PG and Research Department of Mathematics, The Madura College, Madurai, Tamil Nadu, India*
[3] *Department of Mathematics, K. S. Rangasamy College of Technology, Tiruchengode, Tamil Nadu, India*
[4] *Department of Mathematics, Tshwane University of Technology, Pretoria, South Africa*

Abstract. Green nanotechnology offers sustainable solutions to global issues by producing metal oxide nanoparticles with unique properties using eco-friendly methods. Green synthesis using flower extracts is especially promising, as it utilizes natural bio-reducing agents for nanoparticle formation and stabilization. In this study, we investigated the activity of silver nanoparticles synthesized with *Musa Acuminata* flower extract through a novel green procedure. The rapid color change due to the addition of the aqueous extract to the silver nitrate solution confirmed the reduction of Ag^+ ions to Ag nanoparticles. The photocatalytic efficiency of these green-synthesized nanoparticles was evaluated under solar radiation for degrading methyl orange, resulting in up to 90% degradation within 300 minutes. The UV–Vis spectrum verified the formation of nanoparticles, with an absorbance band at 430 nm. This study extends the experimental findings by applying fractional mathematical modeling using the Caputo fractional derivative. The Sumudu Decomposition Method (SDM) was employed to obtain numerical solutions for the proposed model. The boundedness, existence, and uniqueness theorems validate the reliability of the model. Numerical simulations demonstrated the model's accuracy and consistency with the experimental data, offering valuable insights into the behavior and effectiveness of green-synthesized nanoparticles in real-world applications.

2020 Mathematics Subject Classifications: 82D80, 33F05, 03H10

Key Words and Phrases: Green synthesis, *Musa acuminata* Flower extract, Mathematical modeling, Caputo's fractional approach, Sumudu decomposition method

*Corresponding author.
DOI: https://doi.org/10.29020/nybg.ejpam.v18i3.6302

Email addresses: dhanabuvi7302@gmail.com (R. Dhanalakshmi), jeevapirc2405@gmail.com (N. Jeeva), kmdharma6902@yahoo.in (K.M. Dharmalingam), kekanaMC@tut.ac.za (M.C. Kekana)

1. Introduction

Nanotechnology involves the design and manipulation of materials at the nanoscale (1–100 nm), where they exhibit distinctive physical, chemical, and biological properties [1]. These nanoscale materials have applications in diverse fields, including medicine, electronics, energy, and environmental science. Nanoparticles, in particular, demonstrate unique characteristics, such as increased surface area, quantum effects, and superior catalytic activity, compared to their bulk forms. Green synthesis is an eco-friendly method for producing nanoparticles that emphasizes sustainability by reducing the reliance on toxic chemicals and energy-intensive processes. This approach adheres to the principles of green chemistry, which focus on minimizing waste, promoting safety, and using environmentally benign substances. Conventional nanoparticle synthesis methods, although effective, often involve hazardous chemicals and produce harmful by-products. In contrast, green synthesis utilizes natural resources such as plant extracts, microorganisms, and enzymes as reducing and stabilizing agents. The integration of green chemistry and nanotechnology has led to the development of green nanotechnology, which aims to minimize the environmental impact of nanoparticle synthesis. This sustainable approach not only reduces the ecological footprint but also improves the biocompatibility of nanoparticles, making them more suitable for applications in medicine, agriculture, and environmental protection [2].

Green synthesis in nanotechnology offers several significant advantages, primarily in terms of environmental sustainability. By reducing the reliance on toxic chemicals and solvents, these methods minimize the production of harmful byproducts, making the process more environmentally friendly. Additionally, many green synthesis techniques utilize natural and renewable resources, making them more cost-effective. Nanoparticles produced using green methods also tend to exhibit better biocompatibility, which is crucial for biomedical applications such as drug delivery and diagnostics. Furthermore, these methods are often more scalable, particularly when using abundant natural resources such as plants and microbes, making them suitable for large-scale production [3–5].

Mathematical modeling is a powerful tool for analyzing complex systems, predicting outcomes, and optimizing solutions [6–10]. By simulating disease transmission, resource distribution, and structural behaviors, these models enhance decision-making and improve efficiency in fields such as public health and engineering [11–15]. In [16], the green synthesis of silver nanoparticles (AgNPs) was demonstrated using Acer oblongifolium plant extract, highlighting their antibacterial and antiproliferative properties, along with their physicochemical characteristics through mathematical modeling. Meanwhile, [17] explored the green synthesis of silver and iron nanoparticles from the Cordia dichotoma plant for the photocatalytic degradation of methyl orange dye, employing a fractional mathematical model to simulate the degradation process effectively.

Fractional derivatives and Caputo's fractional derivatives were used to capture the memory effects and complex non-local interactions in the model dynamics. These derivatives provide a more accurate representation of the model and control measures, allowing for refined predictions and improved model fidelity in the analysis [18]. The Sumudu Decomposition Method (SDM) is an efficient technique for solving fractional differential

equations, offering a systematic approach to break complex equations into simpler components. It utilizes the Sumudu transformation to convert fractional equations into more manageable forms, thereby simplifying the solution process. By combining the Sumudu transformation with the Adomian decomposition method, each term in the series expansion was computed, enabling independent solutions for each part of the equation. This method is particularly effective for handling nonlinearities and fractional-order terms, providing accurate and efficient solutions. Its ability to handle memory effects and non-local interactions makes it a valuable tool for solving a wide range of fractional problems in applied mathematics and engineering [19–22].

This study explores green synthesis methods for nanoparticle production, including the use of plant extracts and enzymes. The environmental and practical advantages of these methods are discussed, along with their limitations and potential applications in diverse fields such as medicine, agriculture, and environmental science. Silver nanoparticles (AgNPs) [23] have gained significant attention owing to their diverse applications, particularly in agriculture and the pharmaceutical industry. In cancer treatment, AgNPs show promise because they selectively disrupt the mitochondrial respiratory chain, causing reactive oxygen species (ROS) production, which leads to ATP synthesis disruption and DNA damage, thereby inducing apoptosis in cancer cells. One of the key challenges for future applications is the production of large quantities of stable nanoparticles, particularly for medical use. To address this issue, plant-mediated green synthesis methods have emerged as sustainable solutions. These methods utilize plant extracts to synthesize bioactive molecules that are coated with AgNPs, avoiding the use of toxic chemicals. This eco-friendly approach has the potential to produce biocompatible nanoparticles that can be used effectively in cancer therapy and other biomedical applications [24].

2. Experimental Results

2.1. Material Analysis

Silver nitrate was obtained from a chemical laboratory, and deionized water served as the solvent throughout the green synthesis procedure. Flowers of *Musa acuminata* (Red Decca variety) were procured from a local market and used as a natural source for synthesizing silver nanoparticles in this study. The appearance of the *Musa acuminata* flower is shown in Figure 1.

2.2. Preparation of Flower Extract

Fresh, healthy flowers of *Musa acuminata* (Red Decca variety) were obtained from a local market. The flowers were rinsed thoroughly two to three times with distilled water to remove dust and debris and then cut into small sections. Approximately 5 grams of flower pieces were added to 100 mL of distilled water and heated to 80°C for 20 minutes. Afterward, the light brown extract was filtered using Whatman No. 1 filter paper and allowed to cool to room temperature. The prepared extract was then used in subsequent experiments. Figure 2 presents the appearance of the *Musa acuminata* flower extract.

Figure 1: *Musa acuminata* flower

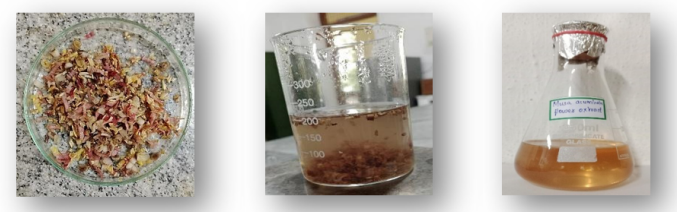

Figure 2: Appearance of the extract

2.3. Preparation of Silver Nitrate Solution

A total of 0.017 grams of silver nitrate ($AgNO_3$) powder was dissolved in 100 mL of distilled water and thoroughly homogenized to ensure uniform mixing. Figure 3 shows the appearance of the reaction mixture.

Figure 3: Appearance of the reaction mixture

2.4. Synthesis of Silver Nanoparticles

A 100 mL solution of $AgNO_3$ was prepared and stirred thoroughly for 20 minutes. Subsequently, 1 mL of the previously prepared flower extract was added, and the solution volume was adjusted to 25 mL. With continuous stirring at room temperature, the solution gradually turned dark brown, indicating the formation of silver nanoparticles (AgNPs) through a reduction reaction. In this experiment, three distinct synthesis conditions were assessed:

(i) 0.5 mL of flower extract combined with 2.5 mL of 1 mM $AgNO_3$ solution (half volume),

(ii) 1 mL of flower extract mixed with 5 mL of 1 mM $AgNO_3$ solution (equal volume),

(iii) 1.5 mL of flower extract with 10 mL of 1 mM $AgNO_3$ solution (double volume).

The flower extract alone (without $AgNO_3$) was used as a control sample. All solutions were incubated in the dark at room temperature for 24–48 hours. Figure 4 depicts the synthesis of silver nanoparticles.

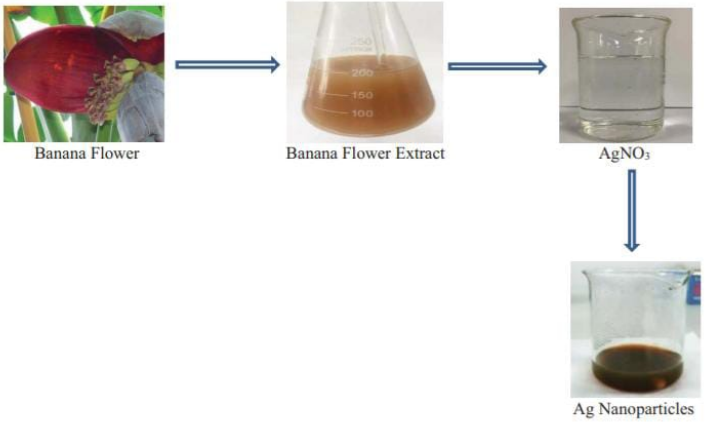

Figure 4: Synthesize of silver nanoparticles

2.5. Ultraviolet Characteristics

Figure 5 displays the UV–visible absorption spectra of silver nanoparticles (AgNPs) synthesized using different volumes (0.5, 1, and 1.5 mL) of *Musa acuminata* extract. The production of AgNPs during the reduction reaction was evidenced by a color shift in the solution from clear to dark brown, indicating the surface plasmon resonance (SPR) effect. This SPR phenomenon occurs when the free electrons in the metal nanoparticles resonate with the incoming light, creating a distinctive SPR absorption band. The peaks in the absorption spectra further validate the SPR effect specific to the AgNPs. The spectra revealed a gradual decline in absorbance, along with a shift in wavelength from 430 to 424

nm and a decrease in intensity. An intensified plasmon band suggests a narrowing of the spectral width [25]. The UV–visible analysis underscores the critical role of silver nitrate ($AgNO_3$) and bioactive compounds in the *Musa acuminata* extract in the synthesis of silver nanoparticles. Increasing the extract concentration resulted in a higher absorbance intensity. Interestingly, the plasmon peak at 424 nm shifted toward shorter wavelengths (blue shift) with higher extract volumes, potentially due to changes in nanoparticle size and morphology [26, 27]. According to Njagi et al. [28], this absorption band, located within the 400–450 nm range, corresponds to the excitation of surface plasmon oscillations in the colloidal silver nanoparticles.

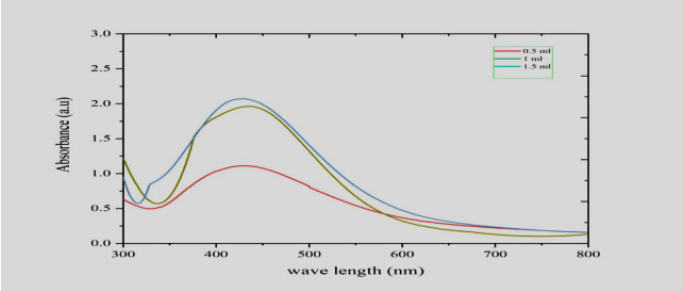

Figure 5: UV-vis absorption spectra of Ag NPs synthesized by a *Musa acuminata* extract

2.6. Fourier Transform Infrared

Fourier-transform infrared (FTIR) spectroscopy was utilized to identify the phytochemicals present in the flower extract and in the silver nanoparticle (AgNP) solution, potentially aiding in the synthesis process. The FTIR analysis detected multiple functional groups based on characteristic absorption bands. The FTIR spectrum of AgNPs synthesized from the flower extract, as illustrated in Figure 6, highlights significant peaks. The bands at 3443 cm^{-1} and 2924 cm^{-1} are indicative of N-H/O-H stretching and the symmetric vibrations of methylene groups, respectively. A peak at 1636 cm^{-1} is associated with the C-N stretching vibration of arene compounds [29]. A pronounced peak at 1528 cm^{-1} corresponds to amide I stretching and suggests interactions between silver ions and carboxylate groups. The strong band at 1384.55 cm^{-1}, linked to C=C stretching in aromatic structures, suggests the presence of flavonoids [30]. Additionally, the peak at 1056 cm^{-1} corresponds to C-N stretching in amines, ether linkages, and aliphatic amines. These biomolecules are integral to the reduction, stabilization, and capping processes during AgNP synthesis.

2.7. Antibacterial Activity

The zone of inhibition values for the synthesized silver nanoparticles (AgNPs) were measured against Escherichia coli (Gram-negative) and Staphylococcus aureus (Gram-positive). According to Patra and Baek [30], multiple potential mechanisms explain the antibacterial activity of AgNPs, including enzyme degradation, inactivation of essential

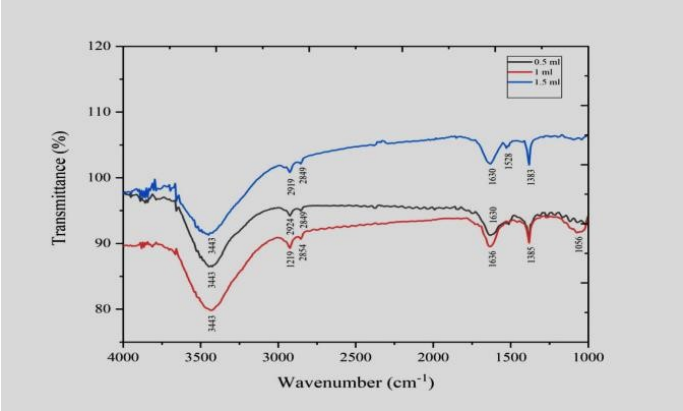

Figure 6: FTIR absorption peaks of Ag NPs synthesized by *Musa acuminata* extract

cellular proteins, and genetic material damage. When compared to Haytham's study [31], which examined the green synthesis of AgNPs using banana peel extract, larger zones of inhibition were observed for E. coli (Gram-negative) than for S. aureus (Gram-positive). Similarly, Alvakonda [32] reported that AgNPs synthesized from banana flower extract exhibited strong antimicrobial activity against multidrug-resistant human pathogens, including S. aureus and E. coli. Haytham [33] also noted that the superior antimicrobial properties of AgNPs are due to their extensive surface area, allowing for greater contact with the cell walls of microorganisms. The zones of inhibition around the bacterial colonies were attributed to the release of diffusible inhibitory compounds from the silver nanoparticles. These biosynthesized AgNPs are extensively used in applications such as cancer therapy, wound healing, antimicrobial treatments, water paints, cotton fabrics, textiles, and more. The green synthesis of AgNPs has opened up new and promising avenues in medicine. The antibacterial Ag silver nanoparticles synthesized with *Musa acuminata* extract are shown in Figure 7. Tables 1 and 2 show the Antibiotic Sensitivity of Various Organisms and the Antibiotic Sensitivity of Various Organisms with 6 MP and Ag 6 MP, respectively.

Table 1: Antibiotic Sensitivity of Various Organisms

SL.No.	**Organism Name**	**Standard Disc**	**Ag**
1	*Escherichia coli*	AK-20mm	10mm
2	*Klebsiella oxytoca*	AK-18mm	Nil
3	*Staphylococcus aureus*	AK-20mm	10mm
4	*Staphylococcus epidermidis*	AK-18mm	08mm

2.8. Degradation Study of Methyl Blue Dye

The Photocatalytic activity (PCA) of the synthesized AgNPs was evaluated using methylene blue (MB) as a model dye. Under sunlight, approximately 90% of the dye was degraded after 300 minutes. The green-synthesized AgNPs possessed a large surface

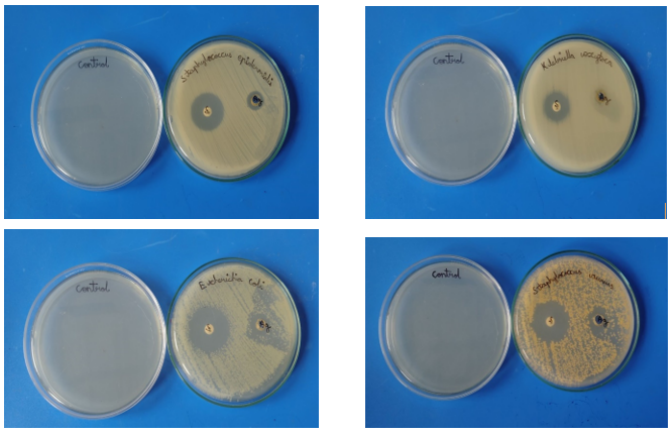

Figure 7: Antibacterial activity of Ag NPs synthesized by *Musa acuminata* extract

Table 2: Antibiotic Sensitivity of Various Organisms with 6 MP and Ag 6 MP

SL.No.	**Organism Name**	**Standard Disc**	**6 MP**	**Ag 6 MP**
1	*Escherichia coli*	AK-20mm	22mm	15mm
2	*Klebsiella oxytoca*	AK-18mm	08mm	10mm
3	*Staphylococcus aureus*	AK-20mm	08mm	12mm
4	*Staphylococcus epidermidis*	AK-20mm	15mm	08mm

area, allowing more MB molecules to interact with the catalyst, thereby enhancing the photocatalytic degradation rate. Upon exposure to light, the MB dye solution generates electron (e^-) and hole (h^+) pairs, as electrons transition from the valence band (VB) to the conduction band (CB), leaving holes in the VB. These holes react with OH^- ions in the solution to form hydroxyl radicals ($OH\cdot$), whereas the electrons interact with dissolved O_2, producing superoxide radicals ($O_2\cdot^-$). These reactive radicals then break down the MB dye molecules into smaller fragments, facilitating the overall degradation process. Figure 8 illustrates the photocatalytic activity of silver nanoparticles synthesized using *Musa acuminata* extract.

3. Mathematical Formation of Green Synthesis Method

In this section, we mathematically model the system's dynamics using differential equations, detailing interactions and degradation rates within five primary compartments.
1. Precursor Silver Ions (S):

$$\frac{dS(t)}{dt} = \Psi - \gamma S(t)P(t) - \varrho S(t)$$

where Ψ is the inflow rate of silver ions, γ is the reaction rate between silver ions and the plant extract $P(t)$, and ϱ represents the natural degradation of silver ions.
2. Intermediates (E):

Figure 8: Photocatalytic activity

$$\frac{dE(t)}{dt} = \gamma S(t)P(t) - \sigma E(t) - \varrho E(t)$$

where γ is the rate at which silver ions transition into intermediates, σ is the rate of formation of silver nanoparticles from intermediates, and ϱ accounts for the degradation of intermediates.

3. Fully Formed Silver Nanoparticles (I):

$$\frac{dI(t)}{dt} = \sigma E(t) - \varrho I(t)$$

where σ represents the rate of nanoparticle formation and ϱ is the degradation rate of silver nanoparticles.

4. Plant Extract (P):

$$\frac{dP(t)}{dt} = -\omega S(t)P(t) - \varphi P(t)$$

where ω is the efficiency of the plant extract in forming intermediates and nanoparticles and φ is the depletion rate of the plant extract as it is consumed in the synthesis process.

5. Degraded Silver (D):

$$\frac{dD(t)}{dt} = \varrho S(t) + \varrho E(t) + \varrho I(t)$$

where ϱ accounts for the degradation of the precursor silver ions, intermediates, and silver nanoparticles.

The governing system of equations of the model (1) captures the dynamics of the green

synthesis of Ag silver nanoparticles using *Musa acuminata* flower extract.

$$\begin{aligned}
\frac{dS(t)}{dt} &= \Psi - \gamma S(t)P(t) - \varrho S(t) \\
\frac{dE(t)}{dt} &= \gamma S(t)P(t) - \sigma E(t) - \varrho E(t) \\
\frac{dI(t)}{dt} &= \sigma E(t) - \varrho I(t) \\
\frac{dP(t)}{dt} &= -\omega S(t)P(t) - \varphi P(t) \\
\frac{dD(t)}{dt} &= \varrho S(t) + \varrho E(t) + \varrho I(t) \\
S(0) = m_1, \quad E(0) &= m_2, \quad I(0) = m_3, \quad P(0) = m_4, \quad D(0) = m_5.
\end{aligned} \tag{1}$$

The precursor silver ions ($S(t)$) interact with the plant extract ($P(t)$), forming intermediates ($E(t)$), which eventually convert into fully developed silver nanoparticles ($I(t)$). The plant extract plays a dual role as both a reducing and stabilizing agent, facilitating nanoparticle formation while being consumed in the process. The degradation rates (ϱ) account for the loss of silver ions, intermediates, and nanoparticles due to oxidation or environmental effects. The parameters Ψ, γ, σ, ω, and φ define the interaction dynamics and control the synthesis efficiency of the silver nanoparticles.

Table 3: Model parameters and description

Parameter	**Description**
Ψ	Rate at which precursor silver ions (Ag^+) are introduced into the system
γ	Interaction rate between precursor silver ions S and plant extract P to form intermediates E
σ	Rate at which intermediates E transform into fully developed silver nanoparticles I
ϱ	Natural degradation rate of silver ions, intermediates, or nanoparticles due to oxidation or environmental factors
φ	Depletion rate of plant extract agents involved in nanoparticle formation
ω	Efficiency rate of the plant extract P in facilitating the formation of AgNPs

3.1. Boundedness Analysis

Positivity and Invariant Region of the Model

(Positivity) [34, 35]: Let $\Omega = \{(S, E, I, P, D) \in \mathbb{R}^5_+ : S(0) > 0, E(0) \geq 0, I(0) \geq 0, P(0) > 0, D(0) \geq 0\}$. Then, the solutions of $\{S(t), E(t), I(t), P(t), D(t)\}$ are all positive

for $t \geq 0$. We consider the first equation of the system (1):

$$\frac{dS(t)}{dt} = \Psi - \gamma S(t)P(t) - \varrho S(t)$$

This gives:

$$\frac{dS(t)}{dt} \geq -\varrho S(t)$$

By separating the variables:

$$\frac{dS}{S} \geq -\varrho\, dt$$

Integrating both sides from 0 to t:

$$\int \frac{dS}{S} \geq \int -\varrho\, dt$$

This results in:

$$\ln S \geq -\varrho t + \ln S(0)$$

The exponential function is applied to both sides:

$$S(t) \geq S(0)e^{-\varrho t}$$

Similarly, applying the same technique to all other state variables E, I, P, and D, proves the lemma $\Omega = \left\{(S, E, I, P, D) \in \mathbb{R}^5_+ : S, E, I, P, D \geq 0\right\}$, ensuring the positivity of all state variables in the system.

(Invariant region) [34, 35]: All solutions $S(t), E(t), I(t), P(t), D(t)$ of the model system are bounded in the region Ω. To analyze the boundedness of the system (1), we define the total concentration $N(t)$ as:

$$N(t) = S(t) + E(t) + I(t) + P(t) + D(t).$$

By taking the derivative with respect to time ($t \geq 0$) and simplifying, we obtain

$$\frac{dN(t)}{dt} \leq \Psi - \varrho N(t).$$

Integrating and further simplification lead us to

$$\lim_{t\to\infty} \sup N \leq \frac{\Psi}{\varrho}.$$

Hence, the total concentration $N(t)$ is bounded above and approaches the value $\frac{\Psi}{\varrho}$ as $t \to \infty$:

$$\Omega = \left\{(S, E, I, P, D) \in \mathbb{R}^5_+ : 0 \leq N \leq \frac{\Psi}{\varrho}\right\}.$$

4. Caputo's Fractional Approach

In this section, we utilize Caputo's fractional approach, reformulating model (1) into fractional-order differential equations (2) to capture the system dynamics more accurately, as follows:

$$\begin{aligned}
\mathcal{F}_t^{\kappa} S(t) &= \Psi - \gamma S(t)P(t) - \varrho S(t) \\
\mathcal{F}_t^{\kappa} E(t) &= \gamma S(t)P(t) - \sigma E(t) - \varrho E(t) \\
\mathcal{F}_t^{\kappa} I(t) &= \sigma E(t) - \varrho I(t) \\
\mathcal{F}_t^{\kappa} P(t) &= -\omega S(t)P(t) - \varphi P(t) \\
\mathcal{F}_t^{\kappa} D(t) &= \varrho S(t) + \varrho E(t) + \varrho I(t)
\end{aligned} \tag{2}$$

where $\mathcal{F}_t^{\kappa}$ is the Caputo's derivative of fractional order and κ is the fractional time derivative

4.1. Existence and Uniqueness

A key question is whether the constructed model accurately represents a physical phenomenon. To validate this, we employ fixed-point theory, demonstrating the existence of a solution for the model as follows:
To analyze the right-hand side of model (2), we apply the operator $\mathcal{C}_t^{\kappa}$ on both sides, yielding

$$\begin{aligned}
S(t) &= S(0) + \mathcal{C}_t^{\kappa}\left[\Psi - \gamma S(t)P(t) - \varrho S(t)\right], \\
E(t) &= E(0) + \mathcal{C}_t^{\kappa}\left[\gamma S(t)P(t) - \sigma E(t) - \varrho E(t)\right], \\
I(t) &= I(0) + \mathcal{C}_t^{\kappa}\left[\sigma E(t) - \varrho I(t)\right], \\
P(t) &= P(0) + \mathcal{C}_t^{\kappa}\left[-\omega S(t)P(t) - \varphi P(t)\right], \\
D(t) &= D(0) + \mathcal{C}_t^{\kappa}\left[\varrho S(t) + \varrho E(t) + \varrho I(t)\right].
\end{aligned}$$

Considering the above equations, we define:

$$U(t) = \begin{pmatrix} S(t) \\ E(t) \\ I(t) \\ P(t) \\ D(t) \end{pmatrix}, \quad U_0(t) = \begin{pmatrix} S(0) \\ E(0) \\ I(0) \\ P(0) \\ D(0) \end{pmatrix}.$$

Let $\Psi(t, U(t))$ represent the functions on the right-hand side of the equations, defined as:

$$\Psi(t, U(t)) = \begin{pmatrix} \Psi - \gamma S(t)P(t) - \varrho S(t) \\ \gamma S(t)P(t) - \sigma E(t) - \varrho E(t) \\ \sigma E(t) - \varrho I(t) \\ -\omega S(t)P(t) - \varphi P(t) \\ \varrho S(t) + \varrho E(t) + \varrho I(t) \end{pmatrix}.$$

The supremum norms are defined as follows:

$$B_i = \sup_{t \in [t-d, t+d]} \|\Psi_i(t, S, E, I, P, D)\|, \quad \text{for } i = 1, 2, 3, 4, 5,$$

and let $C[d, b_i] = [t-d, t+d] \times [u-c_i, u+c_i] = D \times D_i$ for $i = 1, 2, 3, 4, 5$. We define a norm on $C[d, b_i]$ as:

$$\|U(t)\|_\infty = \sup_{t \in [t-d, t+d]} |U(t)|.$$

Consider the Picard operator $\theta : C(D, D_1, D_2, D_3, D_4, D_5) \to C(D, D_1, D_2, D_3, D_4, D_5)$ given by:

$$\theta U(t) = U_0(t) + \int_0^t \Psi(s, U(s))ds.$$

Suppose the solutions of the model are bounded within a time period, i.e.,

$$\|U\| \leq \max\{d_1, d_2, d_3, d_4, d_5\}.$$

Assuming $d = 1 + \sigma t_0 M(\sigma)$, where $B = \max\{B_i\}$ for $i = 1, 2, 3, 4, 5$ and $t_0 = \max\{t \in D\}$, we analyze the following:

$$\|\theta U(t) - U_0(t)\| \leq \frac{1-\sigma}{M(\sigma)} \sup_{t \in D} |\Psi(t, U(t))| + \frac{\sigma}{M(\sigma)} \int_0^t \Psi(s, U(s))ds \leq (1 + \sigma(t_0 - 1))\, B < d,$$

which satisfies $d < d_B$. Now, considering the inequality:

$$\|\theta U_1 - \theta U_2\| = \sup_{t \in D} |U_1 - U_2|,$$

we have:

$$\|\theta U_1 - \theta U_2\| \leq \frac{1-\sigma}{M(\sigma)} k_1 \|U_1 - U_2\| + \frac{\sigma}{M(\sigma)} k_1 \int_0^t \|U_1(s) - U_2(s)\| ds \leq k_1 d \|U_1 - U_2\|,$$

where $k_1 < 1$. Since Ψ is a contraction, it follows that $k_1 d < 1$. Therefore, the operator θ is a contraction, ensuring that the model in (2) has a unique solution.

5. Sumudu Decomposition Method

The Sumudu decomposition is a mathematical technique commonly applied to simplify complex differential equations, particularly in engineering and applied sciences. By transforming functions into more manageable forms, it facilitates the analysis and solution of differential equations, including those involving fractional calculus [19–22].

5.1. Sumudu Transform Basics

Let $F(u)$ denote the Sumudu transform of the function $f(t)$. Then, the Sumudu transform of the Caputo fractional derivative of $f(t)$ of order α can be represented as:

$$S[cD^\alpha f(t)] = u^{-\alpha} \left(F(u) - \sum_{k=0}^{n-1} u^k f^{(k)}(0) \right), \quad n-1 < \alpha < n.$$

The fundamental properties of the Sumudu transform are as follows:

(i) $S[1] = 1$

(ii) $S[t] = u$

(iii) $S[t^{n-1}] = u^{n-1}\Gamma(n), \quad n \in \mathbb{R}^+$

These foundational transformations provide a basis for applying the Sumudu method to more complex functions and systems in fractional calculus and beyond.

5.2. Appication of SDM to Green Synthesis Model

In this subsection, we apply the Sumudu decomposition method (SDM) for the fractional model (2). Considering the Sumudu transform for the system with the corresponding initial conditions, we obtain

$$\begin{aligned} S(t) &= m_1 + \mathcal{S}^{-1}\left[u^{\kappa}\mathcal{S}\left[\Psi - \gamma SP - \varrho S)\right]\right] \\ E(t) &= m_2 + \mathcal{S}^{-1}\left[u^{\kappa}\mathcal{S}\left[\gamma SP - (\sigma+\varrho)E\right]\right] \\ I(t) &= m_3 + \mathcal{S}^{-1}\left[u^{\kappa}\mathcal{S}\left[\sigma E - \varrho I)\right]\right] \\ P(t) &= m_4 + \mathcal{S}^{-1}\left[u^{\kappa}\mathcal{S}\left[-\omega SP - \varphi P\right]\right] \\ D(t) &= m_5 + \mathcal{S}^{-1}\left[u^{\kappa}\mathcal{S}\left[\varrho(S+E+I)\right]\right] \end{aligned} \tag{3}$$

By applying the Adomian polynomial to the nonlinear equation $SP = A$, the general term of the model (3) is derived in a series form and expressed in equation (4).

$$\begin{aligned} \sum_{n=0}^{\infty} S_{n+1}(t) &= m_1 + \mathcal{S}^{-1}\left[u^{\kappa}\mathcal{S}\left[\Psi - \gamma\sum_{n=0}^{\infty} A_n - \varrho\sum_{n=0}^{\infty} S_n)\right]\right] \\ \sum_{n=0}^{\infty} E_{n+1}(t) &= m_2 + \mathcal{S}^{-1}\left[u^{\kappa}\mathcal{S}\left[\gamma\sum_{n=0}^{\infty} A_n - (\sigma+\varrho)\sum_{n=0}^{\infty} E_n\right]\right] \\ \sum_{n=0}^{\infty} I_{n+1}(t) &= m_3 + \mathcal{S}^{-1}\left[u^{\kappa}\mathcal{S}\left[\sigma\sum_{n=0}^{\infty} E_n - \varrho\sum_{n=0}^{\infty} I_n)\right]\right] \\ \sum_{n=0}^{\infty} P_{n+1}(t) &= m_4 + \mathcal{S}^{-1}\left[u^{\kappa}\mathcal{S}\left[-\omega\sum_{n=0}^{\infty} A_n - \varphi\sum_{n=0}^{\infty} P_n\right]\right] \\ \sum_{n=0}^{\infty} D_{n+1}(t) &= m_5 + \mathcal{S}^{-1}\left[u^{\kappa}\mathcal{S}\left[\varrho(\sum_{n=0}^{\infty} S_n + \sum_{n=0}^{\infty} E_n + \sum_{n=0}^{\infty} I_n)\right]\right] \end{aligned} \tag{4}$$

The solutions for S, E, I, P, and D can be represented as infinite series. Given the initial conditions, the initial iteration is obtained as follows:

$$S_0 = m_1, \quad E_0 = m_2, \quad I_0 = m_3, \quad P_0 = m_4, \quad D_0 = m_5. \tag{5}$$

When $n = 0$, by equating both sides of the system of equation (4), we obtain:

$$\begin{aligned}
S_1 &= \mathcal{S}^{-1}\left[u^{\kappa}\mathcal{S}\left[\Psi - \gamma A_0 - \varrho S_0)\right]\right] \\
&= \left[\Psi - \gamma m_1 m_4 - \varrho m_1\right]\frac{t^{\kappa}}{\Gamma(\kappa+1)} \\
E_1 &= \mathcal{S}^{-1}\left[u^{\kappa}\mathcal{S}\left[\gamma A_0 - (\sigma+\varrho)E_0\right]\right] \\
&= \left[\gamma m_1 m_4 - (\sigma+\varrho)m_2\right]\frac{t^{\kappa}}{\Gamma(\kappa+1)} \\
I_1 &= \mathcal{S}^{-1}\left[u^{\kappa}\mathcal{S}\left[\sigma E_0 - \varrho I_0)\right]\right] \\
&= \left[\sigma m_2 - \varrho m_3)\right]\frac{t^{\kappa}}{\Gamma(\kappa+1)} \\
P_1 &= \mathcal{S}^{-1}\left[u^{\kappa}\mathcal{S}\left[-\omega A_0 - \varphi P_0\right]\right] \\
&= \left[-\omega m_1 m_4 - \varphi m_4\right]\frac{t^{\kappa}}{\Gamma(\kappa+1)} \\
D_1 &= \mathcal{S}^{-1}\left[u^{\kappa}\mathcal{S}\left[\varrho(S_0 + E_0 + I_0)\right]\right] \\
&= \left[\varrho(m_1 + m_2 + m_3)\right]\frac{t^{\kappa}}{\Gamma(\kappa+1)}
\end{aligned} \tag{6}$$

When $n = 1$, by equating both sides of the system of equation (4), we obtain:

$$\begin{aligned}
S_2 &= \mathcal{S}^{-1}\left[u^{\kappa}\mathcal{S}\left[\Psi - \gamma A_1 - \varrho S_1)\right]\right] \\
&= \Psi\frac{t^{\kappa}}{\Gamma(\kappa+1)} - \left[\gamma m_1(-\omega m_1 m_4 - \varphi m_4) + \gamma m_4(\Psi - \gamma m_1 m_4 - \varrho m_1) + \varrho(\Psi - \gamma m_1 m_4 - \varrho m_1)\right]\frac{t^{2\kappa}}{\Gamma(2\kappa+1)} \\
E_2 &= \mathcal{S}^{-1}\left[u^{\kappa}\mathcal{S}\left[\gamma A_1 - (\sigma+\varrho)E_1\right]\right] \\
&= \left[\gamma m_1(-\omega m_1 m_4 - \varphi m_4) + \gamma m_4(\Psi - \gamma m_1 m_4 - \varrho m_1) - (\sigma+\varrho)(\gamma m_1 m_4 - (\sigma+\varrho)m_2)\right]\frac{t^{2\kappa}}{\Gamma(2\kappa+1)} \\
I_2 &= \mathcal{S}^{-1}\left[u^{\kappa}\mathcal{S}\left[\sigma E_1 - \varrho I_1)\right]\right] \\
&= \left[\sigma(\gamma m_1 m_4 - (\sigma+\varrho)m_2) - \varrho(\sigma m_2 - \varrho m_3)\right]\frac{t^{2\kappa}}{\Gamma(2\kappa+1)} \\
P_2 &= \mathcal{S}^{-1}\left[u^{\kappa}\mathcal{S}\left[-\omega A_1 - \varphi P_1\right]\right] \\
&= -\left[\omega m_1(-\omega m_1 m_4 - \varphi m_4) + \omega m_4(\Psi - \gamma m_1 m_4 - \varrho m_1) + \varphi(-\omega m_1 m_4 - \varphi m_4)\right]\frac{t^{2\kappa}}{\Gamma(2\kappa+1)} \\
D_2 &= \mathcal{S}^{-1}\left[u^{\kappa}\mathcal{S}\left[\varrho(S_1 + E_1 + I_1)\right]\right] \\
&= \left[\varrho((\Psi - \gamma m_1 m_4 - \varrho m_1) + (\gamma m_1 m_4 - (\sigma+\varrho)m_2) + (\sigma m_2 - \varrho m_3))\right]\frac{t^{2\kappa}}{\Gamma(2\kappa+1)}
\end{aligned} \tag{7}$$

By following this approach, one can obtain the results by adding the equations (5), (6), (7), and so on:

$$\begin{aligned} S(t) &= S_0 + S_1 + S_2 + \cdots \\ E(t) &= E_0 + E_1 + E_2 + \cdots \\ I(t) &= I_0 + I_1 + I_2 + \cdots \\ P(t) &= P_0 + P_1 + P_2 + \cdots \\ D(t) &= D_0 + D_1 + D_2 + \cdots \end{aligned} \tag{8}$$

Therefore, by applying the Sumudu Decomposition Method (SDM), we have derived an approximate solution for the green synthesis model. This approach simplifies the complex system of equations, providing an iterative solution that closely approximates the behavior of the system under study. The resulting approximation can be used to analyze and predict the dynamics of the green synthesis process with greater accuracy and efficiency.

6. Numerical Simulation and Discussion of Results

This section presents the numerical simulations conducted to explore the dynamics of the proposed model over a specified time period. The primary aim is to analyze and visualize the behavior of the model through graphical representations, allowing for a deeper understanding of the system's evolution. The initial conditions for the system are as follows: The concentration of silver ions at the start is $S(0) = 15$, representing the initial quantity of precursor silver ions. The intermediates are initialized at $E(0) = 5$, indicating the initial number of intermediate species involved in the synthesis process. The concentration of fully formed silver nanoparticles is set to $I(0) = 2$, reflecting the initial presence of nanoparticles. The initial concentration of plant extract agents is $P(0) = 10$, which plays a crucial role in the synthesis process. Finally, the initial amount of degraded silver is $D(0) = 1$, representing the initial level of silver that has undergone degradation. Thus this simulation is initialized with the following initial values: $S(0) = 15$, $E(0) = 5$, $I(0) = 2$, $P(0) = 10$, and $D(0) = 1$, which are carefully chosen to represent a realistic starting point for the model. The parameter values used in the simulation are: $\Psi = 5$, $\gamma = 3$, $\sigma = 0.5$, $\varrho = 0.1$, $\varphi = 0.6$, and $\omega = 0.4$, which reflect plausible values for the parameters based on previous studies and theoretical assumptions. The fractional order κ in the model has been varied between 0.6 and 1 for each compartment, offering valuable insights into the influence of fractional calculus on the system's dynamics. By adjusting κ to values of 0.6, 0.7, 0.8, 0.9, and 1, the model reveals different behaviors across compartments. Figure 9 illustrates the variation in the density of Precursor Silver Ions under different values of the fractional order κ. The results indicate a clear trend, where the density of S(t) increases as κ rises, highlighting the influence of the fractional order on the system's behavior over time. Figure 10 illustrates the variation in the density of Intermediates under different values of the fractional order κ. The results indicate a clear trend, where the density of E(t) decreases as κ rises. Figures 11, 12, and 13 illustrates the variation in the density of Fully Formed Silver Nanoparticles, Plant Extract, and Degraded Silver under different values of the fractional order κ respectively. The results indicate a clear trend, where the

density of I(t), D(t), and P(t) increases as κ rises. These findings, as illustrated in Figures 9, 10, 11, 12, and, 13 emphasize the role of fractional derivatives in refining the model's accuracy and demonstrating the complex behavior of the green synthesis process under varying fractional orders. This suggests that κ plays a significant role in modulating the dynamics of silver ions during the synthesis process.

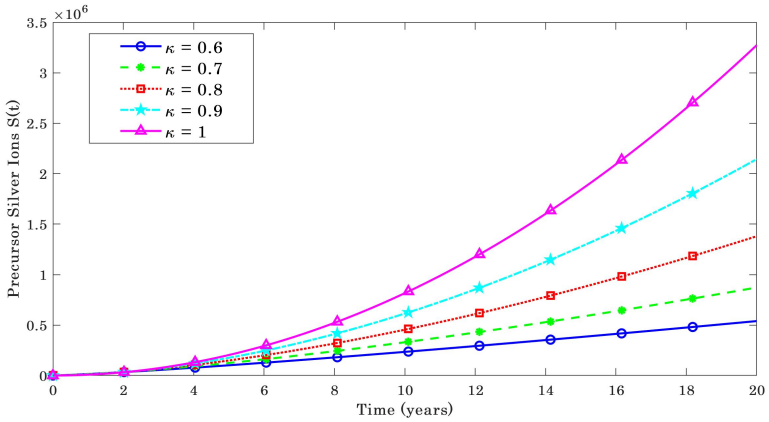

Figure 9: Pictorial representation of numerical solution for precursor silver ions, $S(t)$ class in a time t for different κ

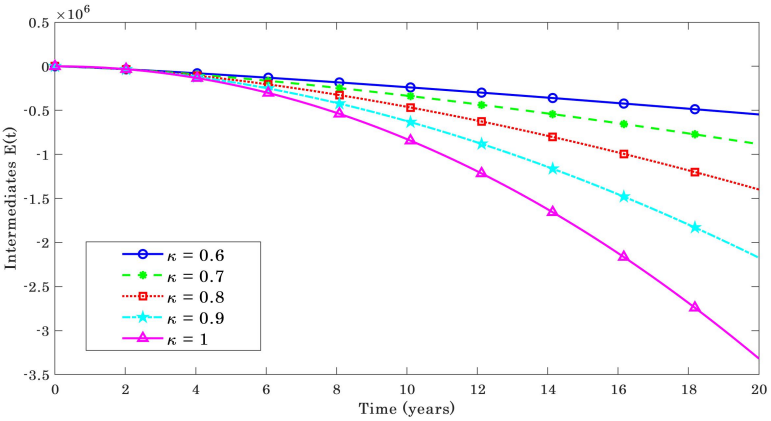

Figure 10: Pictorial representation of numerical solution for intermediates, $E(t)$ class in a time t for different κ

7. Conclusion

The green synthesis method utilizing flower extract from a medicinal plant, such as *Musa acuminata*, offers a cost-effective and eco-friendly alternative to traditional chemical synthesis, eliminating the need for toxic chemical-reducing agents. This approach allows for the production of silver nanoparticles (AgNPs) at room temperature, with *Musa acuminata* flower extract serving as both the reducing and stabilizing agents. The

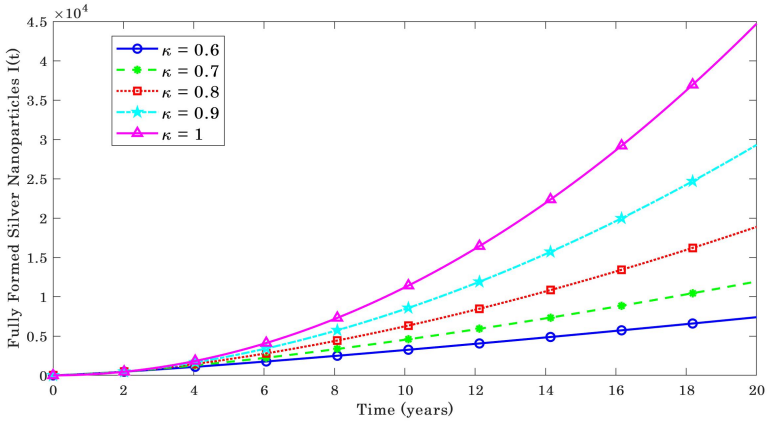

Figure 11: Pictorial representation of numerical solution for fully formed silver nanoparticles, $I(t)$ class in a time t for different κ

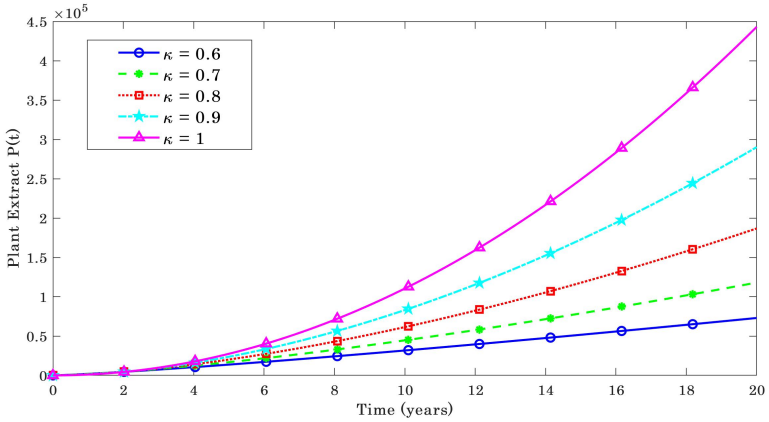

Figure 12: Pictorial representation of numerical solution for plant extract, $P(t)$ class in a time t for different κ

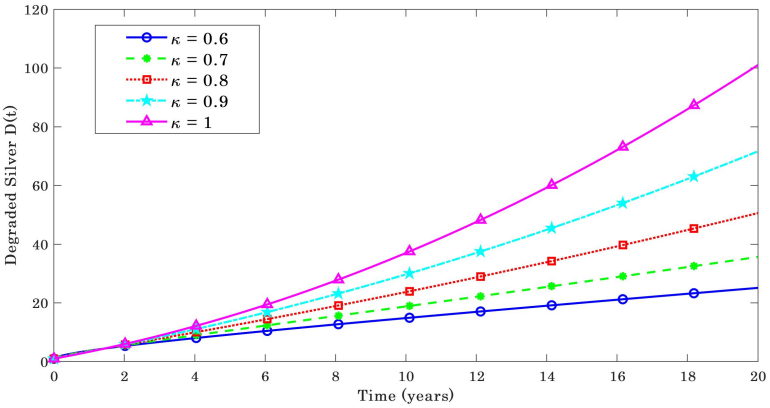

Figure 13: Pictorial representation of numerical solution for degraded silver, $D(t)$ class in a time t for different κ

synthesized AgNPs were characterized using UV–Vis, FTIR, antibacterial analysis, and photocatalytic activity. FTIR and UV–Vis results confirmed the successful formation of nanoparticles. The biosynthesized AgNPs demonstrated significant antibacterial activity against various bacteria, including *E. coli*, *Klebsiella oxytoca*, *Staphylococcus aureus*, and *Staphylococcus epidermidis*. These findings highlight the potential of AgNPs synthesized with *Musa acuminata* flower extract as effective antibacterial and catalytic agents. On a larger scale, green-synthesized AgNPs can be applied in wastewater treatment, environmental remediation, and various bacteria-targeted biological applications.

Furthermore, we mathematically model the entire green synthesis process, incorporating the Caputo fractional approach to capture the dynamics of the system with greater accuracy. By applying this approach, we account for the inherent complexities and memory effects in the system, which are often overlooked in traditional integer order models. We then solved the resulting fractional-order differential equations using the Sumudu Decomposition Method, a powerful analytical tool that allowed us to decompose the system into a series of manageable terms. This method not only provides a more efficient way to solve the model but also aids in understanding the interactions between the various compartments involved in nanoparticle synthesis. To enhance the silver nanoparticle synthesis process, optimizing the reaction parameters such as silver ion inflow rate (Ψ), plant extract concentration, and reaction efficiency (γ, σ) is crucial. Additionally, minimizing degradation rates (ϱ) through stabilization strategies can improve the nanoparticle yield and quality. The combination of these advanced experimental and computational techniques has allowed us to analyze and visualize the behavior of the silver nanoparticles at different stages of the synthesis process. By integrating the mathematical model with experimental results, we gained a deeper understanding of the factors influencing nanoparticle formation, stability, and effectiveness. This approach paves the way for optimizing the synthesis process and provides valuable insights into the potential applications of AgNPs in diverse fields, including environmental remediation, medical treatment, and industrial catalysis.

References

[1] M. Doble and A.K. Kruthiventi. *Green Chemistry and Engineering*. Academic Press, Cambridge, 2007.

[2] M.D. Bolanle Asiyanbola and W. Soboyejo. Journal of surgical education. *Journal of Surgical Education*, 65:155–161, 2008.

[3] F. Khan, M. Shariq, M. Asif, M. A. Siddiqui, P. Malan, and F. Ahmad. Green nanotechnology: Plant-mediated nanoparticle synthesis and application. *Nanomaterials*, 12(4):673, 2022.

[4] S. Ahmad, S. Munir, N. Zeb, A. Ullah, et al. Green nanotechnology: a review on green synthesis of silver nanoparticles — an ecofriendly approach. *International Journal of Nanomedicine*, 14:5087–5107, 2019.

[5] K. Parveen, V. Banse, and L. Ledwani. Green synthesis of nanoparticles: Their advantages and disadvantages. In *AIP Conference Proceedings*, 2016.

[6] F. M. Mrope and N. Jeeva. Modeling the transmission dynamics of banana bunch top disease in banana plants. *Eurasion Journal of Mathematical and Computer Applications*, 12:73–90, 2024.

[7] N. Jeeva and K. M. Dharmalingam. Numerical analysis and artificial neural networks for solving nonlinear tuberculosis model in seitr framework. *Advanced Theory and Simulations*, 2025. Article ID 2401287.

[8] Ali Raza, Kashif Ali, Sanaullah Sattar, Sunday Emmanuel Fadugba, and N. Jeeva. Mathematical modeling and numerical simulations of influenza transmission dynamics with structured infectious population. *Advanced Theory and Simulations*, 2025. Article ID e00236.

[9] F. M. Mrope, O. J. Kigodi, N. Jeeva, and M. Manivel. Mathematical modeling of the impact of insecticides on the transmission dynamics of maize streak disease. *Modeling Earth Systems and Environment*, 11:264, 2025.

[10] K. M. Dharmalingam, N. Jeeva, and Nazek Alessa. Application of chebyshev polynomial-exponential method and tamini-ansari method in dengue transmission dynamics: A comparative study. *International Journal of Analysis and Applications*, 22:2291–8639, 2024.

[11] N. Jeeva and K. M. Dharmalingam. Sensitivity analysis and semi-analytical solution for analyzing the dynamics of coffee berry disease. *Computer Research and Modeling*, 16(3):731–753, 2024.

[12] F. M. Mrope and N. Jeeva. Modeling the transmission dynamics of banana bunch top disease in banana plants. *Eurasian Journal of Mathematical and Computer Applications*, 12(3):73–90, 2024.

[13] A. Ferdous. An ordinary differential equation model for assessing the impact of lifestyle intervention on type 2 diabetes epidemic. *Healthcare Analytics*, 4:100271, 2023.

[14] I. Cooper, A. Mondal, and C.G. Antonopoulos. A sir model assumption for the spread of covid-19 in different communities. *Chaos, Solitons & Fractals*, 139:110057, 2020.

[15] S. Rezapour, H. Mohammadi, and A. Jajarmi. A new mathematical model for zika virus transmission. *Advances in Difference Equations*, page 589, 2020.

[16] S. Dave, A.M. Khan, S.D. Purohit, and D.L. Suthar. Application of green synthesized metal nanoparticles in the photocatalytic degradation of dyes and its mathematical modelling using the caputo–fabrizio fractional derivative without the singular kernel. *Journal of Mathematics*, pages 1–8, 2021.

[17] M. Naveed, B. Bukhari, T. Aziz, S. Zaib, et al. Green synthesis of silver nanoparticles using the plant extract of acer oblongifolium and study of its antibacterial and antiproliferative activity via mathematical approaches. *Molecules*, 27(13):4226, 2022.

[18] M. Caputo and M. Fabrizio. A new definition of fractional derivative without singular kernel. *Progress in Fractional Differential Applications*, 1:73–85, 2015.

[19] G.K. Watugala. Sumudu transform: a new integral transform to solve differential equations and control engineering problems. *International Journal of Mathematical Education in Science and Technology*, 24(1):35–43, 1993.

[20] E. K. Akgül, A. Akgül, and R. T. Alqahtani. A new application of the sumudu

transform for the falling body problem. *Journal of Function Spaces*, pages 1–8, 2021.

[21] R. M. Jena and S. Chakraverty. Analytical solution of bagley-torvik equations using sumudu transformation method. *SN Applied Sciences*, 1(3), 2019.

[22] Q.D. Katatbeh and F.B.M. Belgacem. Applications of the sumudu transform to fractional differential equations. *Nonlinear Studies*, 18(1):99–112, 2011.

[23] M.J. Firdhouse and P. Lalitha. Biosynthesis of silver nanoparticles and its applications. *Journal of Nanotechnology*, pages 1–18, 2015.

[24] M. Muthupandi Kasithevar, M. Muthupandian Saravanan, P. Periyakaruppan Prakash, H. Hema Kumar, M. Muhammad Ovais, H. Hamed Barabadi, and Z.K. Shinwari. Journal of interdisciplinary nanomedicine. *Journal of Interdisciplinary Nanomedicine*, 2(2):131–141, 2017.

[25] W. Zhang, X. Qiao, and J. Chen. Synthesis and characterization of silver nanoparticles in aot microemulsion system. *Chemical Physics*, 330:495–500, 2006.

[26] L. Kelly, E. Coronado, L.L. Zhao, and G.C. Schatz. The optical properties of metal nanoparticles: the influence of size, shape, and dielectric environment. *Journal of Physical Chemistry B*, 107:668–677, 2003.

[27] K.L. Lee and M.A. El-Sayed. Gold and silver nanoparticles in sensing and imaging: sensitivity of plasmon response to size, shape, and metal composition. *Journal of Physical Chemistry B*, 110:19220–19225, 2006.

[28] E.C. Njagi, H. Huang, L. Stafford, H. Genuino, H.M. Galindo, J.B. Collins, G.E. Hoag, and S.L. Suib. Biosynthesis of iron and silver nanoparticles at room temperature using aqueous sorghum bran extracts. *Langmuir*, 27:264–271, 2011.

[29] V. Thiruvengadam and A.V. Bansod. Characterization of silver nanoparticles synthesized using chemical method and its antibacterial property. *Biointerface Research in Applied Chemistry*, 10(6):7257–7264, 2020.

[30] J. Christy, D. Dharaneya, V. Vinmathi, J. Packia, and S. Jacob. Agreen nanobiotechnological approach for the synthesis of silver nanoparticles using the seed coat of tamarindus indica, study of its antibacterial and anticancer activity. *International Journal of Pharmacy and Pharmaceutical Sciences*, 7(1):192–194, 2015.

[31] J.K. Patra and K.H. Baek. Antibacterial activity and synergistic antibacterial potential of biosynthesized silver nanoparticles against foodborne pathogenic bacteria along with its anticandidal and antioxidant effects. *Frontiers in Microbiology*, 8:1–14, 2017.

[32] H.M.M. Ibrahim. Green synthesis and characterization of silver nanoparticles using banana peel extract and their antimicrobial activity against representative microorganisms. *Journal of Radiation Research and Applied Sciences*, 8:265–275, 2015.

[33] N. Alvakonda. Natural synthesis of silver nanoparticles by banana peel extract and as an antibacterial agent. *Journal of Polymer and Textile Engineering*, 3(1):17–25, 2016.

[34] M. Manivel, A. Venkatesh, K. Arunkumar, M. P. Raj, and N. Shyamsunder. A mathematical model of the dynamics of the transmission of monkeypox disease using fractional differential equations. *Advanced Theory and Simulations*, 7, 2024. Article ID 9.

[35] M. Manivel, A. Venkatesh, and S. Kumawat. A comprehensive study of monkeypox disease through fractional mathematical modeling. *Mathematical Modelling and Numerical Simulation With Applications*, 5:65–96, 2025.